Available online at www.sciencedirect.com
ScienceDirect
Biomaterials 28 (2007) 2380–2392
Biomaterials
www.elsevier.com/locate/biomaterials

Review

SPR microscopy and its applications to high-throughput analyses of biomolecular binding events and their kinetics

Charles T. Campbell[a,*], Gibum Kim[b]

[a]*Department of Chemistry, University of Washington, Seattle, Washington 98195-1700, USA*
[b]*Lumera Corporation, 19910 N, Creek Pkwy, suite 100, Bothell, WA 98011, USA*

Received 23 August 2006; accepted 31 January 2007

Abstract

Surface plasmon resonance (SPR) sensing has long been used to study biomolecular binding events and their kinetics in a label-free way. This approach has recently been extended to SPR microscopy, which is an ideal tool for probing large microarrays of biomolecules for their binding interactions with various partners and the kinetics of such binding. Commercial SPR microscopes now make it possible to *simultaneously* monitor binding kinetics on >1300 spots within a protein microarray with a detection limit of ~0.3 ng/cm^2, or <50 fg per spot (<1 million protein molecules) with a time resolution of 1 s, and spot-to-spot reproducibility within a few percent. Such instruments should be capable of high-throughput kinetic studies of the binding of small (~200 Da) ligands onto large protein microarrays. The method is label free and uses orders of magnitude less of the precious biomolecules than standard SPR sensing. It also gives the absolute bound amount and binding stoichiometry.

Keywords: Surface plasmon resonance microscopy; Surface plasmon resonance imaging; Bioaffinity; Kinetics; Protein arrays; DNA arrays

Contents

1. Introduction

Surface plasmon resonance (SPR) spectroscopy is a popular surface analysis method based on changes in the optical reflectivity of a thin metal film (typically gold) when species adsorb or bind to its surface or to any material coated onto its surface. Specifically, it detects with high sensitivity ($<10^{-6}$) and fast time resolution (~1 s) changes in refractive index of any surface coating or solution near the SPR-active metal surface [1–13]. By "SPR spectroscopy", we refer here to measurements of reflectivity both versus wavelength at fixed angle and versus angle at fixed wavelength (also called SPR reflectometry). Functionalization

*Corresponding author. Tel.: +1 206 616 6085; fax: +1 206 616 6250.
E-mail address: campbell@chem.washington.edu (C.T. Campbell).

0142-9612/$ - see front matter © 2007 Elsevier Ltd. All rights reserved.
doi:10.1016/j.biomaterials.2007.01.047

of the metal surface with specific binding sites with bioaffinity creates a biosensor that can detect biomolecular interactions in real time with no labeling requirements. Therefore, SPR spectroscopy has become a common tool in biochemistry and bioanalytical chemistry, especially for determining the on- and off-rates and equilibrium binding constants which describe the interactions between proteins, DNAs or RNAs and a wide variety of other biomolecules or ligands, or for investigating the effects of various cofactors or inhibitors on these binding constants. Many commercial instruments are available for these applications, the most common of which is the Biacore system [14–30]. Our group has studied the kinetics of protein–ligand, protein–dsDNA and protein–vesicle interactions using a home-built SPR spectrometer [8–11].

More recently, SPR microscopy (SPRM), also referred to as "SPR imaging" (SPRI), has started to be used for the same types of measurements, but with high spatial resolution. Since the measurements are done simultaneously over the entire area radiated by the light or imaged onto the detector array (typically a charge-coupled device (CCD) array), combining SPRM with patterned microarrays of biomolecules allows for very high throughput analyses of biomolecular binding. Thus, SPRM has been used to measure the binding of DNAs and RNAs to DNA arrays, of DNA-binding proteins to dsDNA arrays, of proteins to protein and peptide arrays, and even of small ligands to protein arrays. Just like SPR spectroscopy, SPRM can be used for determining the on- and off-rates and equilibrium binding constants of all these types of interactions, only now in high throughput (>1000 interactions simultaneously). Since the amount of biomaterial needed to make one 100 μm spot on an SPR active surface is tiny, and since the same solution can be used to monitor >1000 spots simultaneously, this provides not only a huge savings in time, but also a tremendous cost savings for the precious biomolecules used for these assays. More importantly, since the buffer and temperature and many other variables are exactly the same for each spot in such an analysis, this approach offers an improvement in measurement reliability relative to 1000 independent measurements by the simpler SPR spectroscopy. Table 1 summarizes some of the advantages of SPRM and SPRI for such analyses.

There are several disadvantages shared by both SPR and SPRM. Perhaps the most important is that, without signal amplification in any way, one requires a minimum of ~0.1% of the surface receptors to be occupied to detect their presence. Thus, to achieve the advantages in Table 1, one requires a concentration of the biomolecular binding partner in solution that is at least $K_d/1000$, where K_d is the equilibrium dissociation constant for the interaction of interest. However, a number of methods have been developed for amplification that dramatically relax this limitation, as outlined below. Another disadvantage is that the metal surface must be functionalized with a bioreceptor in a way that avoids non-specific adsorption. Non-specific adsorption can lead to false signals and biosensor fouling. Finally, biomolecules immobilized onto SPR sensor surfaces do not always retain their native bioactivity and, with some immobilization schemes, only a small fraction of the immobilized biomolecules are active. This can effect the determination of binding stoichiometry (biomolecules bound per receptor). The stoichiometry can also be influenced by the proximity of other receptors in the adlayer, especially when the analyte is a large biopolymer [31].

Table 2 lists just a few of the potential applications of SPRM.

Here we will present first a brief review of SPR spectroscopy, and then present a review of SPRM and its applications in microarray-based biaffinity analyses. Because the basis for absolute quantitative analysis in SPRM is the same as that is SPR spectroscopy, we first will present a detailed description of the methods for absolute quantitative analysis in SPR spectroscopy, and explain how these are easily extended to SPRM.

Table 1
Advantages of SPRM for high-throughput bioaffinity assays

- Simultaneous monitoring of rates of >1000 different interactions
- Label-free detection
- *Absolute* quantification of binding amounts and ratios
- Kinetic measurements with ~1 s time resolution
- Detection limit: ~80 fg, or ~1 attomole (<1 million molecules) for 60-kDa proteins
- Can detect small ligands (<300 Da) interacting with >1000 different proteins simultaneously
- Near perfect referencing for removing spurious signals due to changes in index of refraction of buffer solutions, temperature, etc.
- Time response and absolute quantitative nature render analyses of concentrations much more reliable, and make control experiments much easier to design
- Requires much less of the precious biomolecules than normal SPR:
  - On-chip receptors: requires only enough of each for spotting ~1 nL droplet onto microarray
  - Solution-phase biomolecules in the flow cell: requires 1000-fold less, since >1000 interactions probed with every injection to cell
- SPR-active chips typically compatible with inexpensive but reliable robotic spotters
- Timely: many new methods for spotting protein arrays and arrays of other receptors on gold have recently been developed

Table 2
Example potential applications of SPRM for high-throughput bioaffinity analyses

- Analyses of protein and ligand concentrations with protein or antibody arrays
- Analysis of concentrations of DNA-binding proteins from small cell colonies with dsDNA arrays
- Screening for ligands that bind to proteins: drug discovery
- Screening for substrates (peptides) for catalysis by proteases or kinases, and the relative reaction rates of different peptides
- Searches for cofactors in all sorts of protein binding events
- Fundamental research in proteomics, neurobiology, cell biology, …
- Arrays designed for early disease diagnostics, other clinical applications, …

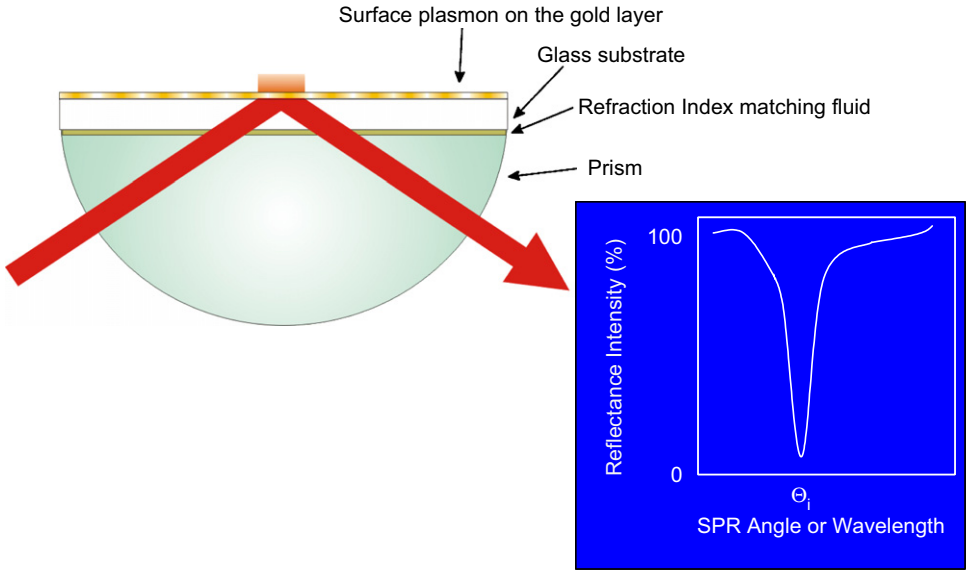

Fig. 1. Schematic of SPR spectroscopy and microscopy. In SPR spectroscopy, a polarized beam of monochromatic light is passed through a prism fitted with a glass slide coated with ~50 nm of gold (or other metal). The light is reflected off the gold, and its intensity is detected at the specular angle, either versus angle at fixed wavelength or, versus wavelength at fixed angle (in which case the monochromator is often positioned after reflection off the gold). The position of the strong minimum that occurs at the SPR resonance condition depends sensitively on the refractive index of the material above and near (<300 nm from) the gold surface, as it is sampled by the evanescent light intensity, which decays exponentially with distance above the gold surface as shown. In SPR microscopy, different regions of the surface are simultaneously probed by a parallel light beam that covers a larger area on the gold surface than shown here. The light is specularly reflected onto a CCD array detector, such that each pixel on the detector array corresponds to a different position on the gold surface.

2. Surface plasmon resonance (SPR) spectroscopy

Typically in SPR spectroscopy, a polarized monochromatic light beam is passed through a prism and its attached, gold-coated glass slide, and reflected off the thin gold coating, which is in contact with the liquid solution of interest (Fig. 1). Excitation of surface plasmons at the gold/solution interface results in nearly complete attenuation of the specularly reflected light intensity for incident angles very near the SPR angle, which depends on wavelength. It can be monitored by following the specularly reflected light intensity versus angle at fixed wavelength or versus wavelength at fixed angle. The position of this sharp resonance "dip" in intensity shifts very sensitively with the index of refraction of the liquid solution in contact with the gold surface and any coatings or adsorbed films on the gold surface. In the situations of interest here, this resonance position is monitored while the solution above the gold is changed using a flow cell, and its shift is proportional to the surface concentration of the species which adsorbs onto the surface from the liquid solution (see below). By monitoring this dip position versus time, SPR spectroscopy thus provides a powerful kinetic technique for interrogating the changes in the surface adsorbed layer on the gold sensor in response to differences in the liquid solutions to which it is exposed. When the gold surface is functionalized with biomolecular receptors, it is a very effective tool for measuring the kinetics and equilibrium constants of bioaffinity interactions (see Fig. 2). It has been employed successfully in thousands of such studies [8–11,14–30].

3. Quantitative SPR spectroscopy: absolute surface concentrations

We have proven that SPR spectroscopy measures an "effective index of refraction", η_{eff}, which is a weighted

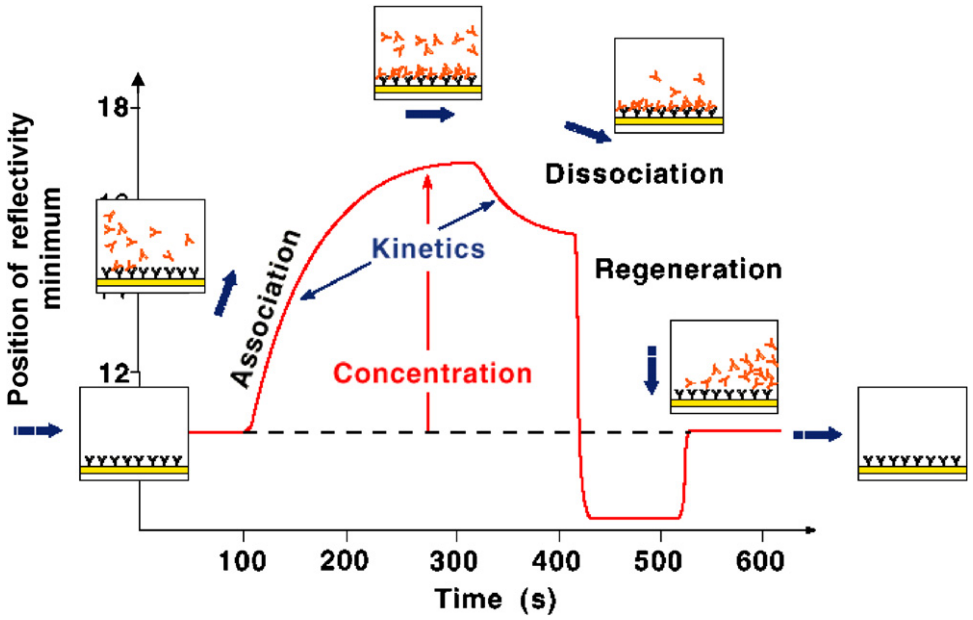

Fig. 2. Schematic of kinetic analyses of bioaffinity interactions using SPR spectroscopy and a gold surface that is functionalized with biomolecular receptors. Adapted from Biacore web site (www.biacore.com).

average of the liquid solution in contact with the gold surface plus any coatings or adsorbed films on the gold surface [8]. We have shown that an SPR system can be calibrated easily with different solutions of known index of refraction (under conditions where the contribution to changes in η_{eff} are dominated by changes in the bulk liquid's refractive index and not by changes in any adsorbed film). After such calibration, any changes in the SPR dip position (i.e., angle or wavelength) versus time can be directly converted into changes in the effective refractive index, with the same units as refractive index [8].

We have also proven that, to a very good approximation under circumstances of interest here, the effective index of refraction is calculated by the average of the index of refraction on the materials (liquid, coatings and adsorbates) in contact with the gold surface, wherein the index of refraction of the material at any distance Z from the gold surface, $\eta(Z)$, is weighted by the factor $\exp(-Z/\lambda)$ in calculating this average as follows [8]:

$$\eta_{\text{eff}} = \int_{Z=0}^{Z=\infty} \eta(Z)\exp(-Z/\lambda)\,\mathrm{d}Z. \tag{1}$$

Note that this factor $\exp(-Z/\lambda)$ is proportional to the intensity of the evanescent light at distance Z from the surface, which decays with a characteristic decay length (λ) given by

$$\lambda = (\lambda_{\text{SPR}}/4\pi)/\text{Re}\{-\eta_{\text{eff}}^4/(\eta_{\text{eff}}^2+\varepsilon_{\text{metal}})\}^{1/2}, \tag{2}$$

where λ_{SPR} is the wavelength of the measurement and $\varepsilon_{\text{metal}}$ is the dielectric constant of solid gold at that wavelength (found tabulated in [32,33]). (Note that λ used here is equal to $l_d/2$ as used in Ref. [8].) Since η_{eff} is directly measured when using a calibrated instrument, everything on the right side of Eq. (2) is known, so that the decay length λ also is known. It is typically ~1/3 of λ_{SPR}, or ~200 nm [8]. Since η_{eff} changes only a few percent in such measurements, we simply use its initial or average value in calculating one λ value applicable for the whole run.

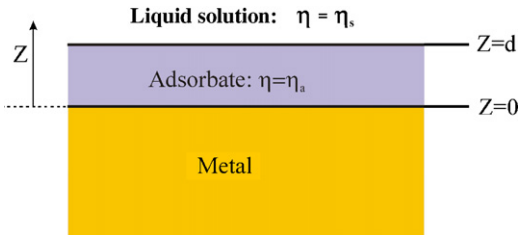

Fig. 3. Schematic of simplified bilayer model for adsorbed layer (a) of thickness d and liquid solution (s) in contact with an SPR-active gold surface.

Eq. (1) has some very simple and useful limits. The most important example occurs for a simple bilayer structure involving an adsorbate a of thickness d and refractive index η_a directly on the metal probe surface, above which is a liquid solution s, of refractive index η_s (Fig. 3). In this case, it reduces to

$$\begin{aligned}\eta_{\text{eff}} &= \eta_a[1-\exp(-d/\lambda)] + \eta_s\exp(-d/\lambda)\\ &= \eta_s + (\eta_a-\eta_s)[1-\exp(-d/\lambda)].\end{aligned} \tag{3}$$

It is typical in the applications described below that $d \ll \lambda$, in which case this simplifies even further to

$$\eta_{\text{eff}} = \eta_s + (\eta_a-\eta_s)(d/\lambda). \tag{4}$$

Thus, the change in η_{eff} upon adsorbing this layer of thickness d is just:

$$\Delta\eta_{\text{eff}} = (\eta_a-\eta_s)(d/\lambda). \tag{5}$$

Thus, the SPR response upon adsorption is proportional to the difference in refractive index between the adsorbate and the solution, $\eta_a - \eta_s$, and the adsorbed layer's thickness, d. Thus, a measurement of $\Delta\eta_{eff}$ upon adsorption using SPR spectroscopy provides the value of d, the adsorbate film thickness. This is used to obtain d from measuring $\Delta\eta_{eff}$.

Note that the above method to measure film thickness, d, also applies when the adsorbate is not spread so nicely in a film of uniform thickness, but instead makes a rough or even porous layer, provided this porosity or roughness occurs on a distance scale (measured parallel to the gold surface) that is small compared to ~5 μm [8]. In that case, the d one obtains is really its "effective thickness", meaning the thickness which this same amount of adsorbate (in mass per unit area) would have if it were spread uniformly at its normal packing density, ρ_a. For this reason, we shall refer to the value of d obtained from using Eq. (5) as d_{eff} throughout the remainder of this paper. Actually, d_{eff} is more interesting than the film's maximum thickness, since it is this effective thickness that must be used to quantify the amount of that adsorbate in mass per unit area [8]. Thus, one applies Eq. (5) to get d_{eff}:

$$d_{eff} = [\Delta\eta_{eff}/(\eta_a - \eta_s)]\lambda \quad (6)$$

and then obtains from d_{eff} the surface concentration:

$$\text{mass per unit area of adsorbate} = d_{eff}\rho_a. \quad (7)$$

In bioanalytical applications, the mass per unit area is the key value of interest. Note that the value of ρ_a used in the above equation must be taken for the same form of matter as that for which η_a is defined.

It is important to know how best to obtain literature values for the needed parameters (η_a and ρ_a) when applying Eqs. (6) and (7). Often the values for the pure bulk materials are known or can be measured. For a molecule like a protein which is not readily obtained in pure form outside of solution, or which may change its charged state when not in aqueous solvent, it is most accurate to use that molecule's so-called "refractive index increment in aqueous buffer" to obtain η_a and its "specific volume in aqueous buffer" (similar to its partial molar volume) to obtain ρ_a (1/specific volume) as described in detail in [8] (see Eq. (10b) therein, and related discussion). These values are tabulated for some biomolecules [34,35], but can also be measured. The key to understanding their use is to remember that the index of refraction of a binary mixture (for example, buffer plus protein, where the complex buffer is treated as a single component for simplicity) is assumed to be given by

$$\eta_{mixture} = \eta_{buffer} f_{buffer} + \eta_{protein} f_{protein}, \quad (8)$$

where f_i is the volume fraction of component i, so that $f_{buffer} = 1 - f_{protein}$. Measurements of the refractive index of a protein–buffer mixture at various protein concentrations allows one to estimate $\eta_{protein}$. The volume fraction of protein is obtained from

$$\rho_{mixture} = \rho_{buffer} f_{buffer} + \rho_{protein} f_{protein}. \quad (9)$$

This same type of analysis has been applied to DNAs, RNAs and many other molecules. Typical resulting values in aqueous buffers are: $\rho_{protein} = 1/0.77\,\text{mL/g} = 1.3\,\text{g/mL}$, $\eta_{protein} = 1.57$ (except for lipo- and glyco-proteins), $\rho_{dsDNA} = 1.7\,\text{g/mL}$ and $\eta_{dsDNA} = 1.7$ [8,34,36–40].

4. SPR microscopy (SPRM) or "SPR imaging" (SPRI)

SPRM, also referred to as SPRI, provides the same type of quantitative data as obtained in biosensing with SPR spectroscopy (i.e., amount adsorbed versus time), but it has the very important added feature of monitoring adsorption with a spatial resolution down to ~4 μm over a large area of a sensing surface [36,41–48].

In most SPR microscopes, an expanded and collimated, polarized and monochromatic light beam (often a He–Ne laser, but sometimes a narrow-pass filtered white light) travels through a prism and an attached glass slide coated with a thin gold film, and reflects from the gold/solution interface at an angle greater than the critical angle [36,41–48]. The reflected light intensity from the illuminated area of the surface is monitored at the specular angle, typically by a CCD detector array. (A more sophisticated commercial version has just been introduced wherein the light is scanned across the sample surface [49].) In any case, each pixel on the CCD array maps into a specific location on the gold surface, and provides the surface information about that spot on the surface (see Fig. 1). The spatial contrast in an SPR microscope image comes from the heterogeneity in the complex dielectric due to differences in refractive index near the surface at different lateral positions across the surface, which results in slight shifts in the resonance angle. This leads to changes across the surface in reflected intensity at an incident angle near the resonance angle. If an adsorbate has a different refractive index than the solvent, its binding to the surface can thus be detected in a spatially resolved way simply by monitoring changes in reflected light intensity at the pixel(s) of interest. Since the pixels on a CCD array are all sampled simultaneously in modern instrumentation, this allows for very high throughput studies of adsorbed amount versus position on the surface, ideally compatible with the probing of microarrays of biomolecules [36,44,46,48,50–68].

A number of designs have been reported for SPR microscopes [36,41–48]. In our home-built SPR microscope [36], a stabilized 632.8 nm HeNe laser serves as the excitation source. The laser beam is p-polarized, expanded and collimated before traveling through an SF14 glass hemi-cylindrical prism and attached glass slide, to illuminate an approximately 16 mm^2 area of the gold-coated slide surface. The reflected light is focused and directed by a lens directly onto the CCD detector of a video camera, creating an image that is automatically digitized by a framegrabber

card and stored using image acquisition software (KSA400, k-Space Associates, Inc., Ann Arbor, MI). The detection optics are connected to an aluminum rail that is attached to a motorized rotation stage. This stage is mounted under an identical stage that holds the prism. The centers of rotation for the two stages are aligned. A computer connected to a stage controller/driver is used to separately and equally vary the angle of incidence and the angle of detection so the CCD detector stays at the specular angle for each angle of incidence. The entire system is mounted on a laser table and covered by a black box to minimize stray light, dust, and airflow effects. The image acquisition software controls the CCD camera exposure time, frame averaging and conversion of measured light intensity values to gray scale levels. A key feature of the software is its ability to integrate the intensity in any number of selected regions of an image simultaneously and plot/store that region's integrated intensity versus time in real time. The fluidics system includes a low-volume (~15 μL) flow cell, a syringe pump, two switching valves, and low dead-volume laminar flow tubing. The syringe is computer controlled for rapid time response in changing this solution in contact with the gold surface (~1 s).

One-dimensional SPRI is a related technique that uses one dimension of the SPR image to measure SPR reflectivity versus frequency and the other dimension to produce a one-dimensional image of the sensor surface [69,70].

5. Quantitative SPR microscopy: absolute surface concentrations with spatial resolution

We now review the method we recently developed for the conversion of light intensities in SPRM (or SPRI) to absolute adsorbate coverages (mass or number of molecules per unit area) [36]. For this purpose, it is best first to set up the angle of light incidence (and detection) of the microscope so that it is operating in the "linear" response region, as defined in Fig. 4. In this range of angles, the change of light intensity is proportional to the change in η_{eff}. The SPR microscope is calibrated easily in much the same way as described above using a series of solvents of different bulk refractive indices, so that changes in reflected light intensity can be converted directly into changes in η_{eff}. A typical calibration plot is shown in Fig. 5. Thereafter, a measurement of the change in light intensity versus time for each spot on the sample surface directly provides $\Delta\eta_{eff}$, which in turn can be used to get d_{eff} (using Eq. (6)) and the mass of adsorbate per unit area (using Eq. (7)), both now measured locally with high spatial resolution.

We have described in detail elsewhere [36] this procedure for microscope calibration and conversion of light intensity changes into mass per unit area. This forms the basis for quantitative analysis using SPRM when absolute bound amounts (mass per unit area) are desired. This procedure has been used in high-throughput bioaffinity analyses using microarrays of both dsDNAs and proteins, to get both the amount of immobilized receptor and the amount of protein bound after exposure to aqueous solution containing that protein [36,66,67]. Comparing these two quantities allowed determination of the receptor–protein binding stoichiometry. Obviously, this can be extended to studies of many other biomolecular pairs.

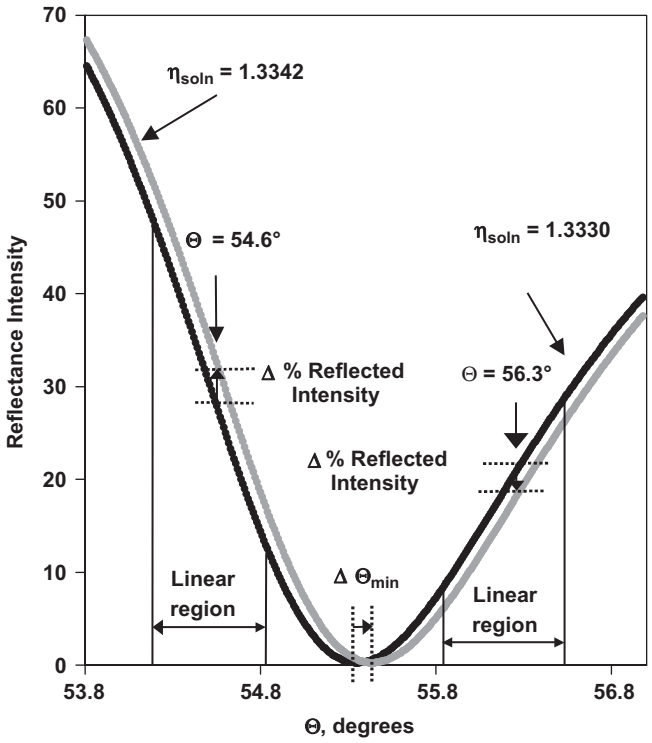

Fig. 4. Principle of SPR microscopy. SPR reflectivity curves versus the light's incident angle (at fixed wavelength) for samples of two different effective refractive indices in contact with the gold surface. There is a linear region on the left where the light intensity increases almost proportionally with the change in effective refractive index over a limited range of ~0.007 refractive index units (equivalent to ~4 ML of adsorbed protein of 50 kDa mass). If the microscope is set up at an angle in this so-called high-contrast region, the intensity change measured at fixed angle is proportional to the change in effective refractive index, which in turn is proportional to adsorbate coverage (or the fractional population of immobilized receptors). From [36].

The *absolute* accuracy of this approach for measuring absolute surface concentrations and binding ratios with SPRM should be better than ±35% [8,36] with, of course, much better precision (< ±5%, see below). Absolute accuracy is typically limited by the accuracy of the parameter η_a (or more properly, $\eta_a - \eta_s$), which often is only known rather approximately.

6. Example applications

SPRM has been investigated as a promising tool for simultaneously monitoring binding events across functionalized surface microarrays. Early work in this arena was pioneered by the research groups of Wolfgang Knoll [41,42,45,68,71–73] and Robert Corn [46,53,74,75]. By creating 1-D or 2-D arrays of binding sites on an

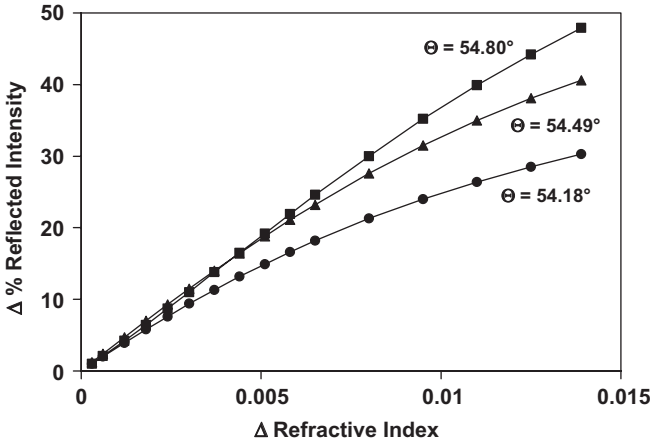

Fig. 5. Calibration plots for an SPR microscope, where the changes in reflected intensity are measured at fixed angle versus changes in bulk refractive index of a simple solution in contact with the gold surface, under conditions where changes in the effective refractive index due to adsorption are negligible. Note that there is a proportional response over a large range (~0.007 refractive index units) when the angle of light incidence is chosen properly to be initially on the right edge of the linear-response region shown in Fig. 4. The variation in the linear regions of the curves with incident angle shows the dependence of the linear dynamic range on proper selection of the high-contrast angle for use in the SPR microscope's measurement. From [36].

SPR-active surfaces, DNA–DNA binding, RNA–DNA binding, protein–DNA binding and other bioploymer interactions have been studied in a parallel fashion by SPRM [36,44,46,48,50–68,76,77]. Some of these applications have been reviewed recently [48].

Corn's group has been very active in the development and characterization of a wide variety of robust surface chemistries to link biological molecules (DNA, proteins, peptides, carbohydrates, RNA, etc.) to gold surfaces, and methods to deposit these in array formats appropriate for high-throughput applications using SPRI [48,50,52,53,56,57,60,61,64,78–81]. Generally, their starting point is a self-assembled monolayer of long-chain alkanethiols that are ω-terminated with an amine functional group, which is then chemically modified with heterobifunctional crosslinkers such as SPDP (*N*-succinimidyl 3-(2-pyridyldithio)-propionamido), SATP (*N*-succinimidyl S-acetylthiopropioate) or SSMCC (sulfosuccinimidyl 4-(*N*-maleimidomethyl) cyclohexane-1-carboxylate). These are then used to chemically attach thiol-modified oligonucleotides or carbohydrates, or cysteine-terminated peptides to the surface.

Corn's group has also demonstrated the application of DNA microarrays for SPRI-based detection of oligonucleotides [46] and ribosomal RNA [50,82], for monitoring the induced formation of hairpin structures [83], as well as for studying the specific binding of two response regulators proteins (OmpR and VanR) to DNA [84]. They have also demonstrated the application of array-based detection with SPRI to quantitatively monitor carbohydrate–protein, peptide–protein, and protein–protein interactions, as well as surface enzyme kinetics [48,55–57,60,62,64,79,81].

Without amplification, the detection limit in SPRI studies of DNA or RNA hybridization onto microarrays was close to 1 nM. Corn's group recently has improved this detection limit by six orders of magnitude to ~1 fM through the use of signal amplification via the enzyme RNase H [63,65]. When a ssDNA target binds to a surface RNA molecule within a single-stranded RNA (ssRNA) microarray, RNase H selectively hydrolyzes the RNA strand in the RNA/DNA heteroduplex, thus releasing the target DNA back into solution. Amplification is achieved since this binding/hydrolysis cycle occurs repeatedly for every DNA molecule, thus removing many surface-bound RNA molecules and rendering the signal decrease observable in SPRI. Yager's group also has used enzymatic amplification in SPRI [85].

Corn's group has recently applied time-resolved SPRI to a number of analyses, including a quantitative analysis of the kinetics of *S*-protein adsorption/desorption onto/from an array composed of five different *S*-peptide variants, and a study the surface enzymatic activities of the protease, factor X_a, with a peptide microarray [64].

We have demonstrated several applications of the method for absolute quantitative measurements described above (i.e., Eqs. (6) and (7)) to time- and spatially-resolved measurements of absolute coverages made with a home-built SPR microscope during protein binding onto gold and onto dsDNA microarrays on gold [36,66,67].

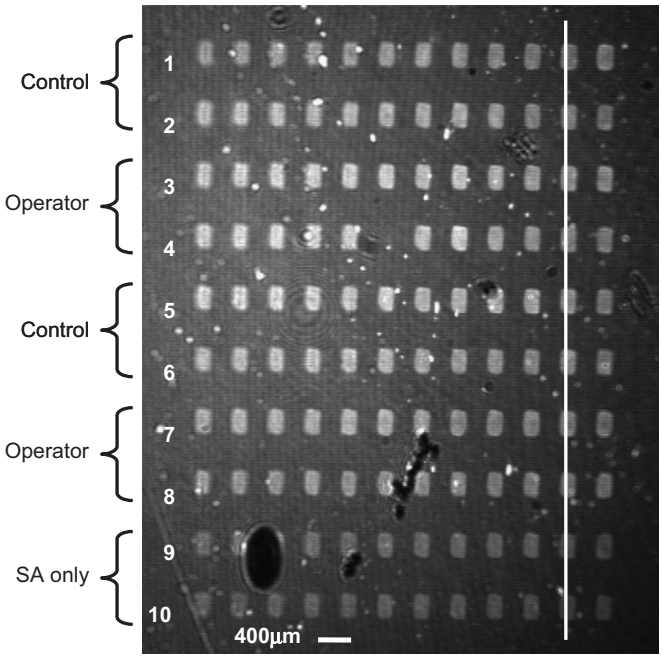

Fig. 6. SPR microscope image and line profile of a section of a 120-spot dsDNA array under buffer solution, before exposure to proteins. The operator spots are those which contain the binding sequence for Gal4, and the control spots are a sequence that is completely unrelated to the Gal4 binding sequence. The "SA only" spots are spots that only have streptavidin, with no added biotinylated dsDNA. The DNAs are ~100 base pairs long, and the spots are 200-μm across. From [66].

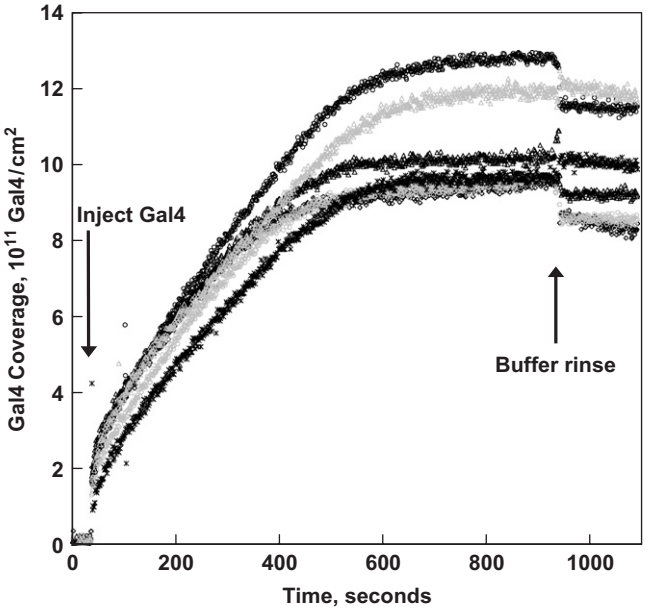

Fig. 7. Simultaneous, real-time measurement of Gal4 binding to (and removal from) six representative, spatially separated spots on the dsDNA array surface, each functionalized with the Gal4 Operator (taken from the 120-spot array shown in Fig. 6). Before Gal4 injection, the surface was in protein-free buffer. The adsorption/removal curves show the SPR response (reflected intensity change, after conversion to surface concentration of Gal4) in each such 200-μm spot, after subtracting the response measured at a nearby Control dsDNA spot, to eliminate signal contributions due to non-specific Gal4 binding and changes in the index of refraction of the buffer solutions. From [66].

For simultaneous measurement of adsorption onto more than one hundred 200 μm × 200 μm spots within a 4 mm × 6 mm area with 1 s time resolution, we demonstrated a detection limit for the change in effective refractive index of $\sim 2 \times 10^{-5}$, or 1.2 ng/cm^2 of protein (0.5 pg in each spot), with a very useful linear dynamic range of ~720 ng/cm^2 of adsorbed protein (~4 close-packed monolayers for a protein with ~50 kDa mass) [36]. We demonstrated its ability for quantitative, real-time measurement of the kinetics of sequence-specific binding of DNA-binding proteins to double-stranded DNA (dsDNA) immobilized in a 10×12 array on a planar gold surface using streptavidin as the surface linker [36,66,67].

Specifically, the binding of the yeast transcription factor Gal4 to a 120-spot dsDNA array made with alternating 200-μm spots of its dsDNA operator sequence and an unrelated DNA sequence proved that this method could be used to simultaneously monitor the kinetics of binding of proteins to 120 different dsDNA sequences with sensitivity to <0.5 pg ($<2 \times 10^7$ molecules) of bound protein in each array spot at a time resolution of 1 s (see Figs. 6 and 7) [66]. Absolute quantitative determination of the binding stoichiometry (i.e., the number of proteins bound per dsDNA) showed the expected saturation ratio of ~two (i.e., it was previously known to bind as a homo-dimer in solution phase) [66]. The data of Fig. 7 show the reproducibility of the response on numerous representative spots with the same DNA sequence. From each spot, an on-rate constant of ~600 Gal4 per dsDNA per s per M of Gal4

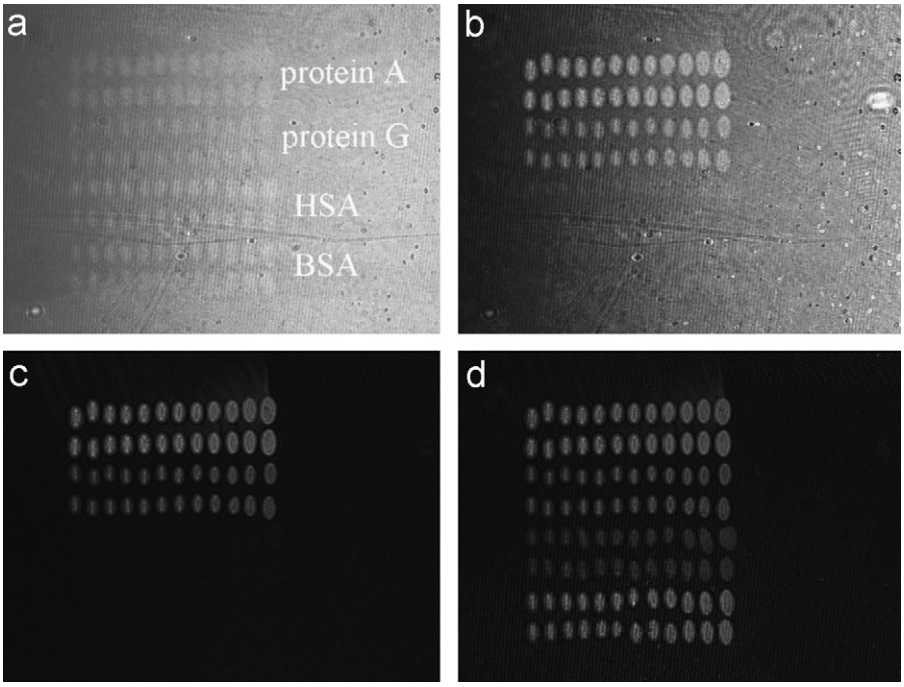

Fig. 8. SPR microscope images of (a) protein microarray, before exposed to antibodies, protein microarray after exposed to 0.1 mg/ml human IgG in PBS, and difference images after exposed to 0.1 mg/ml human IgG in PBS (c) and 0.1 mg anti-BSA IgG in PBS (d). Image (b), (c) and (d) were captured after surface excess antibodies were rinsed with pure PBS. From [86].

concentration was estimated. From longer-time data (not shown but from the long-time behavior of the curves of Fig. 7), the effective first-order off-rate constant for Gal4 binding to its operator sequence was estimated to be $\sim 6.7 \pm 0.7 \times 10^{-5}$ Gal4 homodimers per dsDNA per s. Dividing this by the on-rate constant gave an estimate of the pseudo-first-order equilibrium constant for Gal4 binding to its immobilized Operator sequence of ~200 nM, neglecting the dimeric character of the actual binding [66]. These results demonstrated the feasibility of high-throughput analyses of the kinetics and equilibrium constants of protein–dsDNA binding using SPRM.

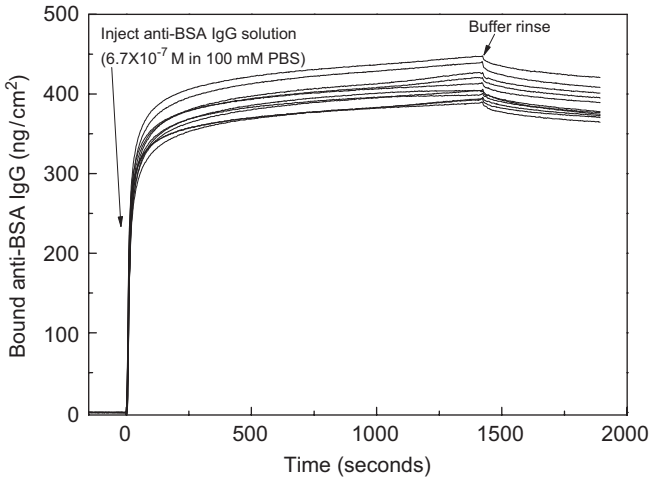

Fig. 9. Representative SPR binding and off-rate curves for ten Protein A spots within a 288-spot array, showing the reproducibility of response to injection of an anti-BSA IgG solution and then a buffer rinse using a SPR microscope developed by the authors.

More recently, we have improved the signal-to-noise ratio of this instrument, and demonstrated that protein arrays can be spotted and probed in this same way. An example of an array for probing antibody–antigen binding is shown in Fig. 8, from [86]. Typical signal-to-noise and reproducibility are shown in Fig. 9. We have proven with this instrument the ability to prepare and probe 300-spot protein arrays, simultaneously detecting each 200-μm spots with 1 s time resolution and a detection limit of 5×10^{-6} refractive index units, corresponding to ~0.4 ng of protein per cm^2, or <80 fg per spot (i.e., ~1 attomole per spot for a 60 kDa biomolecule).

There are now several commercial SPR microscope systems. These include the pioneering instrument partially

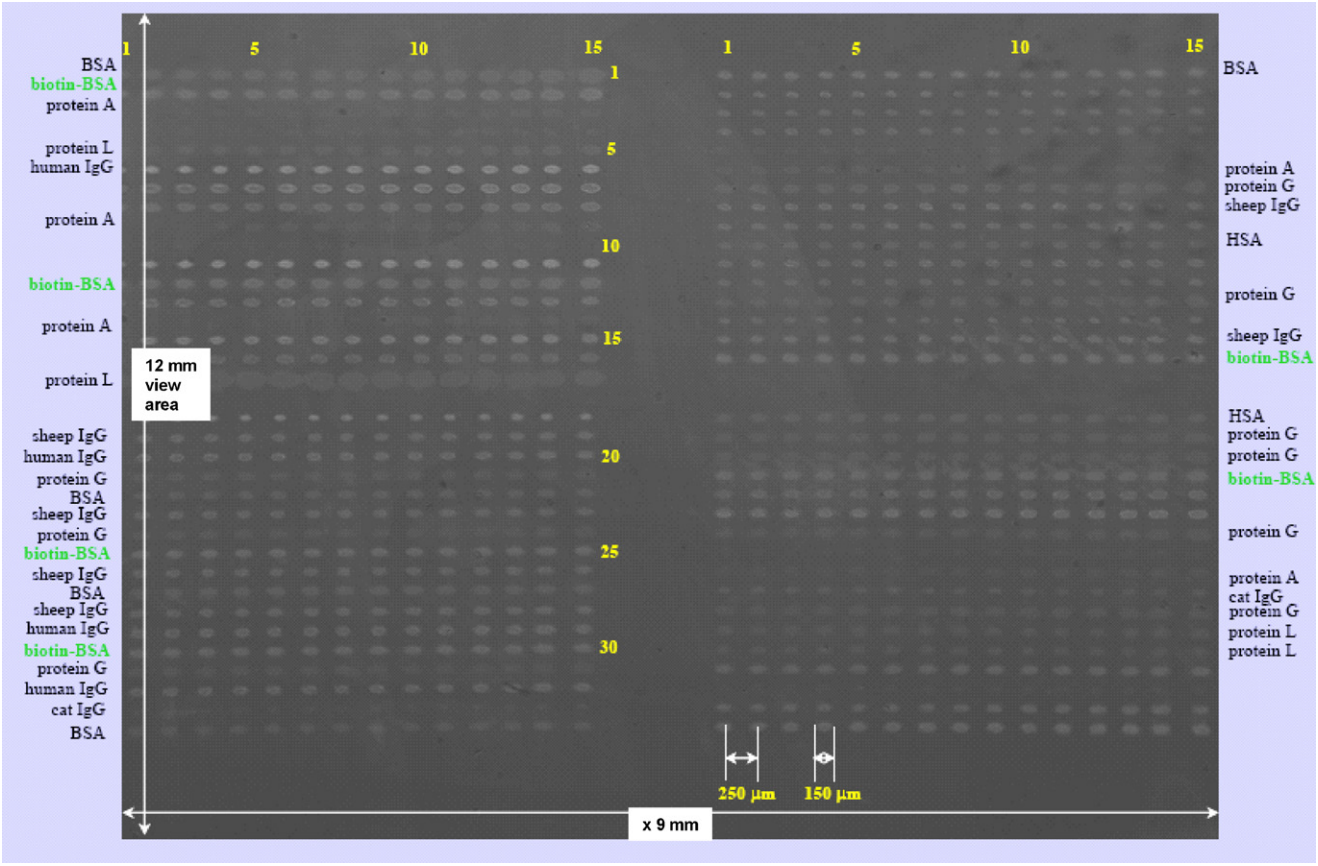

Fig. 10. A 1020-spot protein microarray as imaged by a modern commercial SPR microscope system (Lumera Corp.). The proteins used in this array were: human IgG1, human IgG2, human IgG3, human IgG4, sheep IgG, anti-sheep IgG, human IgG, BSA, ploYclonal anti-BSA, biotin-BSA, lysozyme, HSA, monoclonal HSA, human IgM, cat IgG, protein A, protein L, anti-DNP antibody and monoclonal anti-ovalbumin. The protein spots which showed specific binding (large intensity increases) upon exposure to probe proteins (see below) are labeled on the image. The other protein spots were just control spots, so they are not labeled. From [49].

developed by Robert Corn, and commercialized by GWC Technologies, Inc. (Madison, Wisconsin: http://www.gwctechnologies.com/). Biacore also has developed an instrument (www.biacore.com). These systems are designed for relatively small arrays (10–400 spots).

A commercial SPR microscope system, the Lumera Proteomic Processor (http://www.lumera.com/), was recently developed that handles much larger arrays (1000–10,000 spots) [87]. This instrument has demonstrated the ability to simultaneously monitor binding kinetics on 1350-spot arrays with superb detection limits (~0.3 ng of protein per cm^2, or <50 fg per spot) with a time resolution of 1 s, and even much better spot-to-spot reproducibility than Fig. 9 (10-fold smaller standard deviation in relative bound amounts amongst spots of the same receptor) [49]. That is, it can collect >1000 kinetic curves similar to those in Figs. 2,

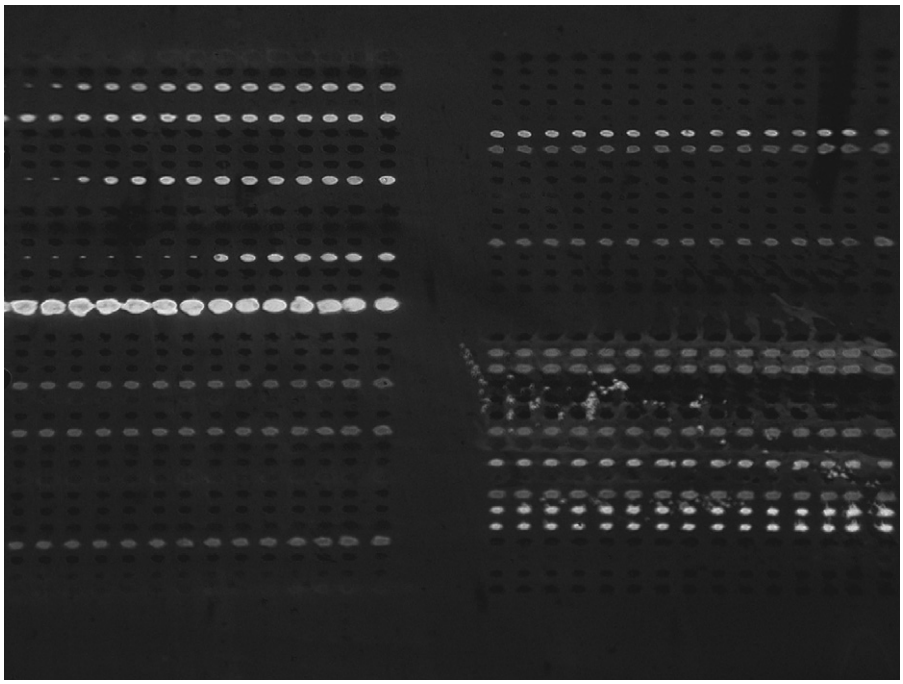

Fig. 11. The same microarray as in Fig. 10 after exposure to human-IgG, presented as a difference image where the intensity shown is only the increase upon exposure to this protein (i.e., after subtraction of the initial intensity before injection). From [49].

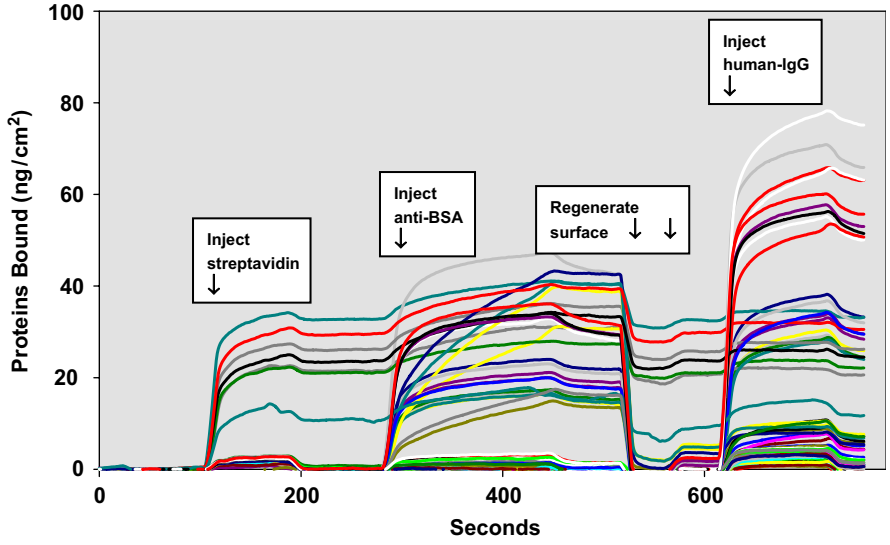

Fig. 12. Example binding curves at some of the spots in the 1020-spot protein microarray of Figs. 10 and 11 after injections of streptavidin, anti-BSA and human IgG (as marked), separated by PBS buffer rinses and one surface regeneration of binding sites by rinsing with a pH 3.2 0.1 M glycine–HCl buffer solution (marked). The expected specificities of binding were observed. This instrument showed detection limits of 0.3 ng/cm^2 (<1 million proteins per spot) while simultaneously monitoring binding kinetics on >1000 spots with 1 s time resolution [49]. This implies that this commercial instrument is capable of monitoring the binding of small ligands (<200 Da) to large protein arrays in this way. From [49].

7 and 9 simultaneously. An example image produced by this instrument of a 1020-spot protein microarray is shown in Fig. 10. In this array, the 20 different proteins were spotted multiple times in rows across the surface. It is clear from these results that, if more proteins had been available at the time, an array of this same size could have been made with 1020 *different* proteins. The difference SPR image of this same array after exposure to human-IgG is shown in Fig. 11, demonstrating the selectivity of binding and detection. A series of kinetic response curves from this array upon injection to solutions of several proteins is shown in Fig. 12. Note the absolute scale on the *y*-axis.

Similar experiments with this Lumera instrument, detecting the binding of a biotinylated peptide of 1500 Da mass (LHRH) onto streptavidin spots within an array of 1200 spots showed a signal >20 times the detection limit [49], implying that this instrument must be capable of probing large protein arrays with small ($\sim$200 Da) ligands in a label-free manner. Successive exposures of a protein array to such ligands should be a powerful tool in drug discovery. This instrument has pattern-recognition software for automatic spot assignments and labeling, which greatly decreases user effort. Its chips are compatible with most commercial robotic spotters or arrayers. The system also has the capability for scaling up to 10,000-spot arrays. Advantages of this scanner include compactness of design and the total absence of diffraction fringes and associated optical problems that arise when using coherent light sources (a diode laser here). This relaxes considerably the demands on lens and sample surface perfection and cleanliness.

As noted above, commercial SPR micrscopes are now capable of detecting less than one million protein molecules binding to a spot in large (1350 spot arrays), while simultaneously monitoring the absolute bound amounts on all spots in the array. A look to the future suggests that SPRM may eventually be converted to a technique that can detect only a single protein molecule binding to such spots in high throughput. This might be done, for example, by labeling the analytes with gold nanoparticles, which would interact strongly with the evanescent wave above the gold surface and should give a greatly amplified response. This would also decrease the minimum detectable concentrations by many orders of magnitude. This has the disadvantage, of course, that it requires labeling, adds complexity and slows down analyte diffusion times.

Acknowledgements

This work was made possible by funding from the Institute for Systems Biology, the University of Washington Center for Nanotechnology, the National Science Foundation, the Department of Energy Office of Basic Energy Sciences, and Lumera Corp. CTC thanks Dr. Ruedi Aebersold, Prof. Jennifer Shumaker-Parry, Dr. Hann Wen Guan, Dr. Pradip Rathod, Dr. Michael Gelb, Dr. Leroy Hood, Prof. Rob Corn and Prof. Wolfgang Knoll for helpful and enjoyable discussions over the years.

References

[1] Lukosz W. Principles and sensitivities of integrated optical and surface plasmon sensors for direct affinity sensing and immunosensing. Biosens Bioelectron 1991;6:215.
[2] Liedberg B, Nylander C, Lundstrom I. Biosensing with surface plasmon resonance—how it all started. Biosens Bioelectron 1995;10:1995.
[3] Hutchinson AM. Evanescent wave biosensors: real-time analysis of biomolecular interactions. Mol Biotechnol 1995;3:47.
[4] Garland PB. Optical evanescent wave methods for the study of biomolecular interactions. Quart Rev Biophys 1996;29:91.
[5] Huber A, Demartis S, Neri D. The use of biosensor technology for the engineering of antibodies and enzymes. J Mol Recog 1999;12:198.
[6] Rabbany SY, Donner BL, Ligler FS. Optical immunosensors. Crit Rev Biomed Eng 1994;22:307.
[7] Jonnson U, Malmqvist M. Real time biospecific interaction analysis: the integration of surface plasmon resonance detection, general biospecific interface, and microfluidics into one analytical system. In: Turner A, editor. Advances in biosensors. San Diego: JAI Press Ltd.; 1992. p. 291.
[8] Jung LS, Campbell CT, Chinowsky TM, Mar M, Yee SS. Quantitative interpretation of the response of surface plasmon resonance sensors to adsorbed films. Langmuir 1998;14:5636–48.
[9] Jung LS, Nelson KE, Campbell CT, Lu HB, Stayton P, Yee SS, et al. SPR measurements of binding and disassociation of wild-type and mutant streptavidin on mixed biotin-containing alkyl-thiolate monolayers. Sensors Actuators 1999;B54:137.
[10] Jung LS, Nelson KE, Stayton PS, Campbell CT. Binding and dissociation kinetics of wild-type and mutant streptavidins on mixed biotin-containing alkylthiolate monolayers. Langmuir 2000;16(24):9421–32.
[11] Jung LS, Shumaker-Parry JS, Campbell CT, Yee SS, Gelb MH. Quantification of tight binding to surface-immobilized phospholipid vesicles using surface plasmon resonance: binding constant of phospholipase A(2). J Am Chem Soc 2000;122(17):4177–84.
[12] Jung LS, Campbell CT. Sticking probabilities in adsorption of alkanethiols from liquid ethanol solution onto gold. J Phys Chem B 2000;104(47):11168–78.
[13] Jung LS, Campbell CT. Sticking probabilities in adsorption from liquid solutions: alkylthiols on gold. Phys Rev Lett 2000;84(22):5164–7.
[14] Wood SJ. DNA DNA hybridization in real-time using Biacore. Microchem J 1993;47(3):330–7.
[15] Malmborg AC, Duenas M, Ohlin M, Soderlind E, Borrebaeck CAK. Selection of binders from phage displayed antibody libraries using the BIAcore(TM) biosensor. J Immunol Methods 1996;198(1):51–7.
[16] Jensen KK, Orum H, Nielsen PE, Norden B. Kinetics for hybridization of peptide nucleic acids (PNA) with DNA and RNA studied with the BIAcore technique. Biochemistry 1997;36(16):5072–7.
[17] Medina MB, VanHouten L, Cooke PH, Tu SI. Real-time analysis of antibody binding interactions with immobilized *E. coli* O157:H7 cells using the BIAcore. Biotechnol Tech 1997;11(3):173–6.
[18] Nieba L, NiebaAxmann SE, Persson A, Hamalainen M, Edebratt F, Hansson A, et al. BIACORE analysis of histidine-tagged proteins using a chelating NTA sensor chip. Anal Biochem 1997;252(2):217–28.
[19] Fivash M, Towler EM, Fisher RJ. BIAcore for macromolecular interaction. Curr Opin Biotechnol 1998;9(1):97–101.
[20] Myszka DG, Jonsen MD, Graves BJ. Equilibrium analysis of high affinity interactions using BIACORE. Anal Biochem 1998;265(2):326–30.

[21] Malmqvist M. BIACORE: an affinity biosensor system for characterization of biomolecular interactions. Biochem Soc Trans 1999; 27(2):335–40.
[22] Myszka DG. Kinetic, equilibrium, and thermodynamic analysis of macromolecular interactions with BIACORE. Method Enzymol 2000;323:325–40.
[23] Rich RL, Myszka DG. BIACORE J: a new platform for routine biomolecular interaction analysis. J Mol Recogn 2001;14(4):223–8.
[24] Abdiche YN, Myszka DG. Probing the mechanism of drug/lipid membrane interactions using Biacore. Anal Biochem 2004;328(2): 233–43.
[25] Cannon MJ, Papalia GA, Navratilova I, Fisher RJ, Roberts LR, Worthy KM, et al. Comparative analyses of a small molecule/enzyme interaction by multiple users of Biacore technology. Anal Biochem 2004;330(1):98–113.
[26] Mistrik P, Moreau F, Allen JM. BiaCore analysis of leptin–leptin receptor interaction: evidence for 1:1 stoichiometry. Anal Biochem 2004;327(2):271–7.
[27] Myszka DG. Analysis of small-molecule interactions using Biacore S51 technology. Anal Biochem 2004;329(2):316–23.
[28] Katsamba PS, Navratilova I, Calderon-Cacia M, Fan L, Thornton K, Zhu MD, et al. Kinetic analysis of a high-affinity antibody/antigen interaction performed by multiple Biacore users. Anal Biochem 2006;352(2):208–21.
[29] Naslund A, Bjorkelund H, Stenberg J, Andersson K, Franklin G. Rapid, reproducible screening of drug compound–target protein interactions using Biacore A100. Nat Methods 2006:14–6.
[30] Safsten P, Klakamp SL, Drake AW, Karlsson R, Myszka DG. Screening antibody–antigen interactions in parallel using Biacore A100. Anal Biochem 2006;353(2):181–90.
[31] Shumaker-Parry JS, Campbell CT, Stormo GD, Silbaq FS, Aebersold RH. Probing protein: DNA interactions using a uniform monolayer of DNA and surface plasmon resonance. In: Proceedings of SPIE photonics west conference, international biomedical optics symposium. San Jose, CA: SPIE; 2000.
[32] Innes RA, Sambles JR. J Phys F: Met Phys 1987;17:277–87.
[33] Palick ED. Handbook of Optical Constants of Solids. Orlando, FL: Academic Press; 1985.
[34] Armstrong Jr SH, Budka MJE, Morrison KC, Hasson M. J Am Chem Soc 1947;69:1747.
[35] Lide DR, editor. CRC handbook of chemistry and physics. 77th ed. Boston: CRC Press, Inc.; 1996.
[36] Shumaker-Parry JS, Campbell CT. Quantitative methods for spatially resolved adsorption/desorption measurements in real time by surface plasmon resonance microscopy. Anal Chem 2004;76(4):907–17.
[37] Darnell JE, Lodish H, Baltimore D. Molecular cell biology. New York: Scientific American Books; 1990.
[38] Leslie TE, Lilley TH. Aqueous-solutions containing amino-acids and peptides. 20. Volumetric behaviour of some terminally substituted amino-acids and peptides at 298.15 K. Biopolymers 1985;24:695–710.
[39] Harrington RE. The flow birefringence of persistence length deoxyribonucleic acid. Hydrodynamic properties, optical anisotropy, and hydration shell anisotropy. J Am Chem Soc 1970;92:6957.
[40] Wu PG, Fujimoto BS, Song L, Schurr JM. Effect of ethidium on the torsion constant of linear and super-coiled DNA. Biophys Chem 1991;41:217.
[41] Rothenhausler B, Knoll W. Surface plasmon microscopy. Nature 1988;332:615.
[42] Knoll W. Interfaces and thin films as seen by bound electromagnetic waves. Annu Rev Phys Chem 1998;49:569.
[43] Berger CEH, Kooyman RPH, Greve J. Resolution in surface plasmon microscopy. Rev Sci Instrum 1994;65:2829.
[44] Zizlsperger M, Knoll W. Multispot parallel on-line monitoring of interfacial binding reactions by surface plasmon microscopy. Prog Colloid Polym Sci 1998;109:244.
[45] Aust EF, Sawodny M, Ito S, Knoll W. Surface plasmon and guided optical wave microscopies. Scanning 1994;16:353.
[46] Thiel AJ, Frutos AG, Jordan CE, Corn RM, Smith LM. In situ surface plasmon resonance imaging detection of DNA hybridization to oligonucleotide arrays on gold surfaces. Anal Chem 1997;69(24): 4948–56.
[47] Lyon LA, Holliway WD, Natan MJ. An improved surface plasmon resonance imaging apparatus. Rev Sci Instrum 1999;70: 2076–81.
[48] Smith EA, Corn RM. Surface plasmon resonance imaging as a tool to monitor biomolecular interactions in an array based format. Appl Spectrosc 2003;57(11):320A–32A.
[49] Guan HW, Kim G, Jiang L, Rathod PK, Campbell CT, Nishimoto A. The proteomics processor: a new system for high-throughput analyses of biomolecular interaction kinetics by SPR microscopy. in preparation.
[50] Nelson BP, Grimsrud TE, Liles MR, Goodman RM, Corn RM. Surface plasmon resonance imaging measurements of DNA and RNA hybridization adsorption onto DNA microarrays. Anal Chem 2001;73(1):1–7.
[51] Brockman JM, Nelson BP, Corn RM. Surface plasmon resonance imaging measurements of ultrathin organic films. Annu Rev Phys Chem 2000;51:41–63.
[52] Brockman JM, Frutos AG, Corn RM. A multistep chemical modification procedure to create DNA arrays on gold surfaces for the study of protein–DNA interactions with surface plasmon resonance imaging. J Am Chem Soc 1999;121(35):8044–51.
[53] Jordan CE, Frutos AG, Thiel AJ, Corn RM. Surface plasmon resonance imaging measurements of DNA hybridization adsorption and streptavidin/DNA multilayer formation at chemically modified gold surfaces. Anal Chem 1997;69(24):4939–47.
[54] Li YA, Wark AW, Lee HJ, Corn RM. Single-nucleotide polymorphism genotyping by nanoparticle-enhanced surface plasmon resonance imaging measurements of surface ligation reactions. Anal Chem 2006; 78(9):3158–64.
[55] Fang S, Lee HJ, Wark AW, Kim HM, Corn RM. Determination of ribonuclease H surface enzyme kinetics by surface plasmon resonance imaging and surface plasmon fluorescence spectroscopy. Anal Chem 2005;77(20):6528–34.
[56] Lee HJ, Li Y, Wark AW, Corn RM. Enzymatically amplified surface plasmon resonance imaging detection of DNA by exonuclease III digestion of DNA microarrays. Anal Chem 2005;77(16): 5096–100.
[57] Wark AW, Lee HJ, Corn RM. Long-range surface plasmon resonance imaging for bioaffinity sensors. Anal Chem 2005;77(13):3904–7.
[58] Frutos AG, Corn RM. SPR of ultrathin organic films. Anal Chem 1998;701:A449.
[59] Nelson BP, Frutos AG, Brockman JM, Corn RM. Near-infrared surface plasmon resonance measurements of ultrathin films. 1. Angle shift and SPR imaging experiments. Anal Chem 1999;71:3928.
[60] Lee HJ, Wark AW, Corn RM. Creating advanced multifunctional biosensors with surface enzymatic transformations. Langmuir 2006;22(12):5241–50.
[61] Lee HJ, Wark AW, Li Y, Corn RM. Fabricating RNA microarrays with RNA–DNA surface ligation chemistry. Anal Chem 2005;77(23): 7832–7.
[62] Lee HJ, Wark AW, Goodrich TT, Fang SP, Corn RM. Surface enzyme kinetics for biopolymer microarrays: a combination of Langmuir and Michaelis–Menten concepts. Langmuir 2005;21(9): 4050–7.
[63] Goodrich TT, Lee HJ, Corn RM. Enzymatically amplified surface plasmon resonance imaging method using RNase H and RNA microarrays for the ultrasensitive detection of nucleic acids. Anal Chem 2004;76(21):6173–8.
[64] Wegner GJ, Wark AW, Lee HJ, Codner E, Saeki T, Fang SP, et al. Real-time surface plasmon resonance imaging measurements for the multiplexed determination of protein adsorption/desorption kinetics and surface enzymatic reactions on peptide microarrays. Anal Chem 2004;76(19):5677–84.

[65] Goodrich TT, Lee HJ, Corn RM. Direct detection of genomic DNA by enzymatically amplified SPR imaging measurements of RNA microarrays. J Am Chem Soc 2004;126(13):4086–7.
[66] Shumaker-Parry JS, Aebersold R, Campbell CT. Parallel, quantitative measurement of protein binding to a 120-element double-stranded DNA array in real time using surface plasmon resonance microscopy. Anal Chem 2004;76(7):2071–82.
[67] Shumaker-Parry JS, Zareie MH, Aebersold R, Campbell CT. Microspotting streptavidin and double-stranded DNA Arrays on gold for high-throughput studies of protein–DNA interactions by surface plasmon resonance microscopy. Anal Chem 2004;76(4): 918–29.
[68] Piscevic D, Lawall R, Veith M, Liley M, Okahata Y, Knoll W. Oligonucleotide hybridization observed by surface-plasmon optical techniques. Appl Surf Sci 1995;90(4):425–36.
[69] O'Brien MJ, Perez-Luna VH, Brueck SRJ, Lopez GP. A surface plasmon resonance array biosensor based on spectroscopic imaging. Biosens Bioelectron 2001;16(1–2):97–108.
[70] Fu E, Ramsey S, Thariani R, Yager P. One-dimensional surface plasmon resonance imaging system using wavelength interrogation. Rev Sci Instrum 2006;77(7).
[71] Hickel W, Knoll W. Surface plasmon optical characterization of lipid monolayers at 5 μm lateral resolution. J Appl Phys 1990;67: 3572.
[72] Haussling L, Ringsdorf H, Schmitt F-J, Knoll W. Biotin-functionalized self-assembled monolayers on gold: surface plasmon optical studies of specific recognition reactions. Langmuir 1991;7:1837.
[73] Fernandez U, Fischer TM, Knoll W. Surface-plasmon microscopy with grating couplers. Opt Commun 1993;102(1–2):49–52.
[74] Frey BL, Jordan CE, Kornguth S, Corn RM. Control of the specific adsorption of proteins onto cold surfaces with poly(L-lysine) monolayers. Anal Chem 1995;67(24):4452–7.
[75] Jordan CE, Corn RM. Surface plasmon resonance imaging measurements of electrostatic biopolymer adsorption onto chemically modified gold surfaces. Anal Chem 1997;69(7):1449–56.
[76] Kambhampati DK, Knoll W. Surface-plasmon optical techniques. Curr Opin Colloid Interface Sci 1999;4(4):273–80.
[77] Kambhampati DK, Jakob TAM, Robertson JW, Cai M, Pemberton JE, Knoll W. Novel silicon dioxide sol-gel films for potential sensor applications: a surface plasmon resonance study. Langmuir 2001;17(4):1169–75.
[78] Wegner GJ, Lee NJ, Marriott G, Corn RM. Fabrication of histidine-tagged fusion protein arrays for surface plasmon resonance imaging studies of protein–protein and protein–DNA interactions. Anal Chem 2003;75(18):4740–6.
[79] Wegner GJ, Lee HJ, Corn RM. Characterization and optimization of peptide arrays for the study of epitope–antibody interactions using surface plasmon resonance imaging. Anal Chem 2002;74(20):5161–8.
[80] Smith EA, Wanat MJ, Cheng YF, Barreira SVP, Frutos AG, Corn RM. Formation, spectroscopic characterization, and application of sulfhydryl-terminated alkanethiol monolayers for the chemical attachment of DNA onto gold surfaces. Langmuir 2001;17(8):2502–7.
[81] Smith EA, Thomas WD, Kiessling LL, Corn RM. Surface plasmon resonance imaging studies of protein–carbohydrate interactions. J Am Chem Soc 2003;125(20):6140–8.
[82] Nelson BP, Liles MR, Frederick KB, Corn RM, Goodman RM. Label-free detection of 16S ribosomal RNA hybridization on reusable DNA arrays using surface plasmon resonance imaging. Environ Microbiol 2002;4(11):735–43.
[83] Smith EA, Kyo M, Kumasawa H, Nakatani K, Saito I, Corn RM. Chemically induced hairpin formation in DNA monolayers. J Am Chem Soc 2002;124(24):6810–1.
[84] Smith EA, Erickson MG, Ulijasz AT, Weisblum B, Corn RM. Surface plasmon resonance imaging of transcription factor proteins: interactions of bacterial response regulators with DNA arrays on gold films. Langmuir 2003;19(5):1486–92.
[85] Hasenbank MS, Fu E, Yager P. Lateral spread of an amplification signal using an enzymatic system on a conductive surface. Langmuir 2006;22(18):7451–3.
[86] Kim G, Jiang L, Rathod PK, Campbell CT, Nishimoto A, Casasanta V. A demonstration of high-throughput immunoassay and small molecule binding on protein microarrays with SPR microscopy. In: NSTI-Nanotech 2005 (Proceedings of the 2005 nano science and technology institute conference). 2005. p. 381–4.
[87] Boozer C, Kim G, Shuxin Cong HGA, Londergan T. Looking towards label-free biomolecular interaction analysis in a high-throughput format: a review of new surface plasmon resonance technologies. Curr Opin Biotechnol 2006;17:1–6.